Druitt, T.H., Kutterolf, S., Ronge, T.A., and the Expedition 398 Scientists
Proceedings of the International Ocean Discovery Program Volume 398
publications.iodp.org

Data report: X-ray fluorescence scanning of Sites U1591 and U1599, IODP Expedition 398, Hellenic Arc Volcanic Field[1]

Thomas A. Ronge,[2,3] Steffen Kutterolf,[2] Tatiana I. Fernandez-Perez,[2] Michael Manga,[2] Abigail Metcalfe,[4] Jonas Preine,[2] Masako Tominaga,[2] Adam Woodhouse,[2] Jesse Yeon,[3] Tim Druitt,[2] Sarah Beethe,[2] Alexis Bernard,[2] Carole Berthod,[2] Hehe Chen,[2] Shun Chiyonobu,[2] Acacia Clark,[2] Susan DeBari,[2] Ralf Gertisser,[2] Christian Hübscher,[2] Raymond M. Johnston,[2] Christopher Jones,[2] K. Batuk Joshi,[2] Günther Kletetschka,[2] Olga Koukousioura,[2] Xiaohui Li,[2] Molly McCanta,[2] Iona McIntosh,[2] Antony Morris,[2] Paraskevi Nomikou,[2] Katharina Pank,[2] Ally Peccia,[2] Paraskevi N. Polymenakou,[2] and Yuzuru Yamamoto[2]

[1] Ronge, T.A., Kutterolf, S., Fernandez-Perez, T.I., Manga, M., Metcalfe, A., Preine, J., Tominaga, M., Woodhouse, A., Yeon, J., Druitt, T., Beethe, S., Bernard, A., Berthod, C., Chen, H., Chiyonobu, S., Clark, A., DeBari, S., Gertisser, R., Hübscher, C., Johnston, R.M., Jones, C., Joshi, K.B., Kletetschka, G., Koukousioura, O., Li, X., McCanta, M., McIntosh, I., Morris, A., Nomikou, P., Pank, K., Peccia, A., Polymenakou, P.N., and Yamamoto, Y., 2024. Data report: X-ray fluorescence scanning of Sites U1591 and U1599, IODP Expedition 398, Hellenic Arc Volcanic Field. In Druitt, T.H., Kutterolf, S., Ronge, T.A., and the Expedition 398 Scientists, Hellenic Arc Volcanic Field. Proceedings of the International Ocean Discovery Program, 398: College Station, TX (International Ocean Discovery Program). https://doi.org/10.14379/iodp.proc.398.204.2024
[2] **Expedition 398 Scientists' affiliations.** Correspondence author: **ronge@iodp.tamu.edu**
[3] Texas A&M University, United States.
[4] Université Clermont Auvergne, France.

Contents

Keywords
International Ocean Discovery Program, IODP, *JOIDES Resolution*, Expedition 398, Hellenic Arc Volcanic Field, Site U1591, Site U1599, X-ray fluorescence core scanning, XRF

References (RIS)

MS 398-204
Received 12 August 2024
Accepted 10 September 2024
Published 12 December 2024

Abstract

International Ocean Discovery Program (IODP) Expedition 398, Hellenic Arc Volcanic Field, recovered volcanic and nonvolcanic sediments and Messinian evaporites, as well as the nonvolcanic basement. The total recovery of about 3.3 km has the potential to significantly expand our understanding of the volcanic and tectonic history of the Christiana-Santorini-Kolumbo volcanic field and the climate history of the eastern Mediterranean. Here we report semiquantitative bulk elemental analyses of X-ray fluorescence core scans for Site U1591, drilled off Christiani Island, and Site U1599, drilled off Anafi Island, and compare these to records of natural gamma radiation that were measured aboard the R/V *JOIDES Resolution*.

1. Introduction

Approximately 800 million people around the world live in regions that are potentially threatened by volcanic eruptions and related hazards such as ash plumes, pyroclastic flows, earthquakes, and even tsunamis (Loughlin et al., 2015). The Expedition 398 research area in the Christiana-Santorini-Kolumbo volcanic field (CSKVF) is particularly hazardous because the islands of the Aegean Sea are densely populated and host millions of tourists every year. In the past, the CSKVF has produced many often highly explosive eruptions (e.g., Druitt et al., 1999; Druitt and Vougioukalakis, 2019). Expedition 398 data are revealing that the eruptions may be much larger than previously thought (Druitt et al., 2024a; Preine et al., 2024). To better understand the volcanic history of the CSKVF, as well as submarine volcanism in general, Expedition 398 drilled 12 sites (U1589–U1600) in the Aegean Sea (**Druitt et al.**, 2024b). Of these 12 sites, two (U1591 and U1599; Figure **F1**) were selected for downcore analyses of elements to generate a data set of semiquantitative X-ray fluorescence (XRF) measurements (Penkrot et al., 2018; Taylor et al., 2022).

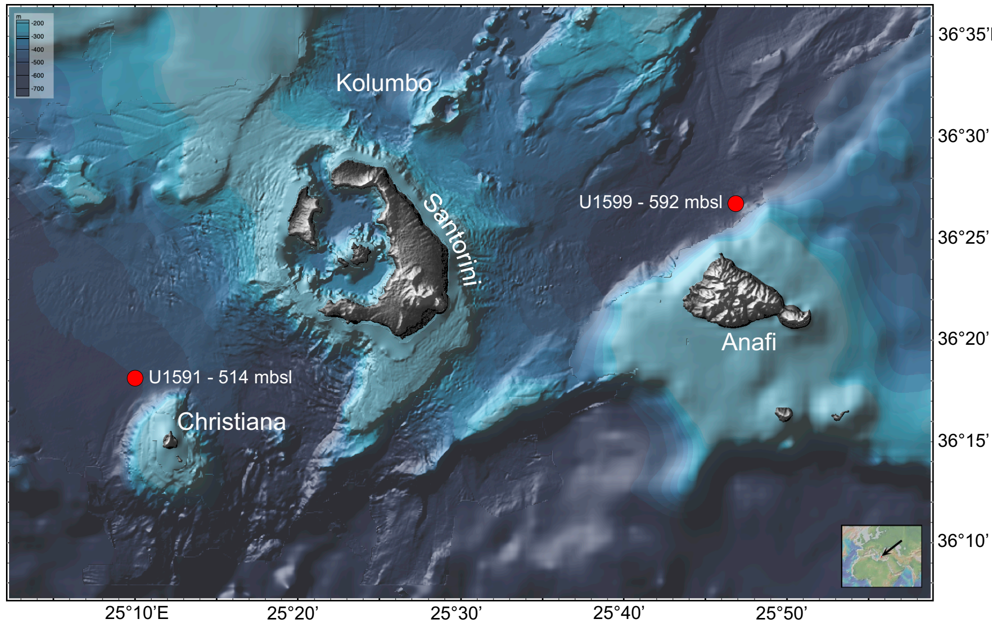

Figure F1. Bathymetric map of the CSKVF with locations of Sites U1591 and U1599. Inset: location map. Created with GeoMapApp (Ryan et al., 2009).

2. Methods and materials

2.1. Drill sites and settings

Expedition 398 Site U1591 is located 514 meters below sea level (mbsl) ~8 km northwest of Christiani Island and ~20 km southwest of Santorini (Hole U1591A: 36°18.7615′N, 025°09.0057′E; Figure **F1**). Three holes (U1591A–U1591C) were drilled to a maximum recovery depth of 902.7 meters below seafloor (**Druitt et al.**, 2024c). Site U1591 targeted the volcano-sedimentary fill of the Christiana Basin, where the fill reaches deeper than in the Anhydros and Anafi Basins and records the earlier history of the CSKVF (Druitt et al., 2024a).

When Expedition 398 began in December 2022, there was no plan to drill at the location that eventually became Site U1599. However, during the expedition, we were able to apply for two new drill sites (U1599 and U1600), and permission to drill was granted by the International Ocean Discovery Program (IODP) Environmental Protection and Safety Panel as well as the Greek authorities. Site U1599 lies in the Anafi Basin (Hole U1599A: 36°26.9592′N, 25°46.8005′E) about 6 km north of Anafi Island at 592 mbsl (**Druitt et al.**, 2024d; Figure **F1**). The site was selected because it consists of (1) a presumably most complete sequence of even lower magnitude volcanic eruptions due to its location downwind from Santorini as well as Kolumbo and (2) a condensed sequence of tephra without quantities of mass-wasting debris (Preine et al., 2022; **Druitt et al.**, 2024d).

2.2. XRF core scanning

At IODP's Gulf Coast Repository (GCR; College Station, Texas, USA), we scanned the archive halves for Sites U1591 (Table **T1A**, **T1B**) and U1599 (Table **T2A**, **T2B**) along the splice (**Druitt et al.**, 2024c; **Druitt et al.**, 2024d) using third- and fourth-generation Avaatech XRF core scanners for Sites U1591 and U1599, respectively. The scanner cross- and downcore slits were set to 12 and 10 mm, respectively. Each section was scanned at two excitement levels: 10 kV to measure major and minor elements (including Al, Ar, Ca, Fe, Mg, P, S, Si, and Ti) and 30 kV to analyze heavier major and minor elements (e.g., Fe, K, Mn, Rb, Sr, Ti, and Zr), both with a count time of 6 s. Where possible, we scanned at a constant increment of 5 cm; however, due to biscuited sediments, some sections were scanned at irregular intervals and contain gaps in the XRF records. To select suitable positions for the scanner to land on, we used a 3D-printed replica of the scanning window to avoid

Table T1A. XRF data shown in this manuscript along the splice of Site U1591. The complete data set can be found in the Laboratory Information Management System database. **Download table in CSV format.**

Table T1B. NGR data shown in this manuscript along the splice of Site U1591. The complete data set can be found in the Laboratory Information Management System database. **Download table in CSV format.**

Table T2A. XRF data shown in this manuscript along the splice of Site U1599. The complete data set can be found in the Laboratory Information Management System database. **Download table in CSV format.**

Table T2B. NGR data shown in this manuscript along the splice of Site U1599. The complete data set can be found in the Laboratory Information Management System database. **Download table in CSV format.**

drilling disturbance, bioturbation, and other unsuitable intervals. We scanned the interval of 186.88–904.86 m on the core composite depth below seafloor (CCSF) depth scale for Site U1591 (**Druitt et al.**, 2024c) and 11.25–686.26 m CCSF for Site U1599 (**Druitt et al.**, 2024d).

To ensure the quality of our scans, standards were run before and after each scanning day, with 20 replicate measurements in the morning and no replicates in the evening. Additionally, we excluded all data points with positive Ar values, as this indicates that the scanner's detector did not sit flush on the core's surface and thus measured ambient air.

2.3. Natural Gamma Radiation Logger scanning

The Natural Gamma Radiation Logger (NGRL) for whole-round cores, designed and built at Texas A&M University (Vasiliev et al., 2011), measures the natural emission resolution of gamma rays from the decay of 238-uranium (^{238}U), 232-thorium (^{232}Th), and 40-potassium (^{40}K). The natural gamma radiation (NGR) detection unit contains 8 NaI scintillator detectors, 7 plastic scintillator detectors, and 22 photomultipliers. The NGRL was calibrated with ^{137}Cs and ^{60}Co sources and identifying peaks at 662 keV (^{137}Cs) and 1330 keV (^{60}Co), using the 1170 keV peak for verification. Reported gamma ray counts were summed over the range of 100–3000 keV. Measurements were made every 10 cm. Intrinsic spatial resolution, defined by the full width at half maximum, was 17 cm, and an edge correction was applied to measurements within 20 cm of the ends of each section (Vasiliev et al., 2011).

3. Results

3.1. Stratigraphic trends

The highly variable nature of the intercalated volcanic and nonvolcanic deposits along the splice (**Druitt et al.**, 2024b) at both sites results in equally variable XRF records for most elements. These can be compared to the continuous NGR record from shipboard core scanning as a tool to monitor variations in clay and volcanic matter variations throughout the stratigraphy on board.

As expected for volcaniclastic and nonvolcanic marine sediments, the XRF counts for Ca and Si are significantly higher than for the majority of other elements (Figures **F2**, **F3**). A pronounced excursion of the Ca, Al, and Si counts and, to a lesser extent, of the grain-size proxy ln(Zr/Rb) (see **ln(Zr/Rb)-derived grain size data**) occurs in a coarser grained lithology at about 566.2 m CCSF for Site U1591 but is absent in the NGR record (Figure **F2**).

At Site U1591, the most noteworthy change throughout all parameters (NGR and XRF) occurs at the transition from the Pliocene (Lithostratigraphic Unit II) to the Miocene (Unit III) (Figure **F2**; Table **T1A**, **T1B**). This transition marks the occurrence of Messinian-age evaporites, in particular laminated and nodular anhydrite (Hsü, 1987), gypsum, and micrite (**Druitt et al.**, 2024c). Being virtually absent for most of Site U1591, sulfur counts increase from values close to 0 in Unit II to almost 800,000 counts in Unit III (Figure **F2**), in good agreement with the anhydrite ($CaSO_4$) and gypsum ($CaSO_4{\cdot}2H_2O$) calcium sulfates identified on board (**Druitt et al.**, 2024c; Figure **F4**).

Evaluating XRF records along the splice of Site U1599 reveals several interesting patterns. At the transition from Lithostratigraphic Unit IV (micrite and calcareous sandstone) to Unit III (dolomitic marl), Fe counts decrease by about 57% from average counts of ~217,000 in Unit IV to ~94,000 in Unit III (Figure **F3**; Table **T2A**, **T2B**). Additionally, throughout all of Unit IV and halfway into Unit III at about 390 m CCSF, the major trends of shipboard NGR and onshore XRF Ca counts are roughly parallel to each other. Both have lower values in Unit IV and the lower half of Unit III, followed by a parallel increase between 486 and 390 m CCSF (Figure **F3**). Between 50.1 and 68.2 m CCSF, Al and Si values are noticeably reduced. This interval corresponds to the loca-

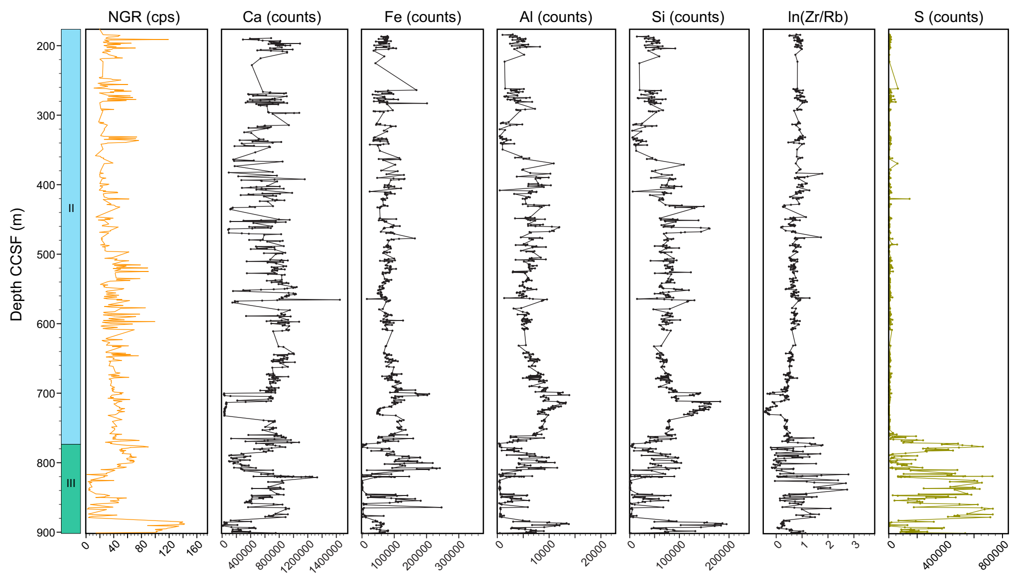

Figure F2. Shipboard spectral NGR and shore-based XRF core scans, Site U1591. Lithostratigraphic units: II = mostly nonvolcanic sediments intercalated with volcanics and tuffaceous deposits, III = evaporites (Druitt et al., 2024c). cps = counts per second.

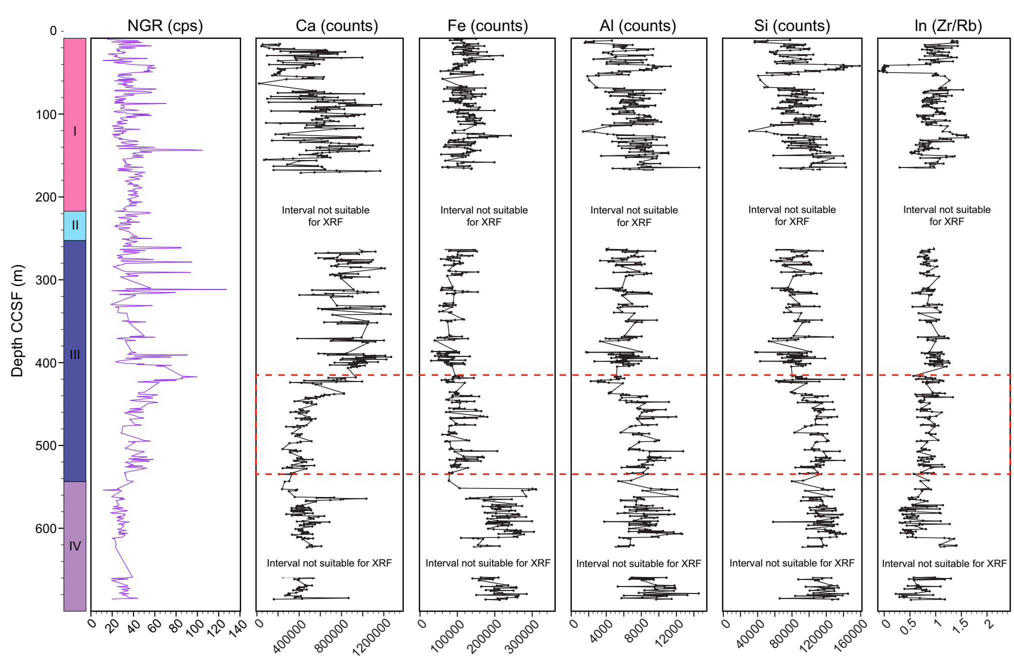

Figure F3. Shipboard spectral NGR and shore-based XRF core scans along the splice, Site U1599. Lithostratigraphic units: I = volcanic/tuffaceous with intercalated nonvolcanic oozes, II = nonvolcanic ooze dominated, III = dolomitic marl, IV = micrite and calcareous sandstone (Druitt et al., 2024d). Dashed box = interval shown in Figure F6. cps = counts per second.

tion of the lapilli-sized Lower Pumice 1 (**Druitt et al.**, 2024b). Note that this interval could not be scanned completely due to the rough surface of the split cores. In the interval between 40.38 and 50.13 m CCSF, ln(Zr/Rb) counts all decline rapidly, with Ca and Fe showing only minor excursions (Figure **F3**). Along the splice, this interval consists of several sections of carbonate oozes and organic-rich oozes (**Druitt et al.**, 2024d).

3.2. Elemental correlation

Owing to the highly variable record of volcanics (ash, pumice, and lithics) and nonvolcanic oozes and marls, the correlation strength between selected elements is expectedly weak and nondiagnostic. We have plotted elements that are indicative of terrigenous and oceanic/pelagic origin against each other (Croudace and Rothwell, 2015). Neither major elements indicative for terrigenous origin (e.g., Si versus Ti and K versus Fe) nor for pelagic origin (e.g., Ca versus Si and Sr versus Ca) show a clear correlation along the entire splice (Figure **F5**).

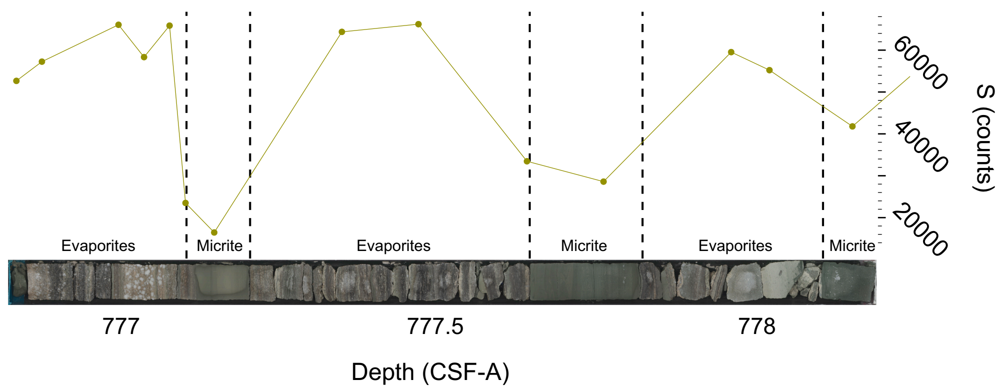

Figure F4. Core photo compared to XRF sulfur counts, Section 398-U1591-59R-1. Dashed lines separate intervals of sulfur-rich evaporites from micrite, as identified in the visual core description, and are in good agreement with the XRF data.

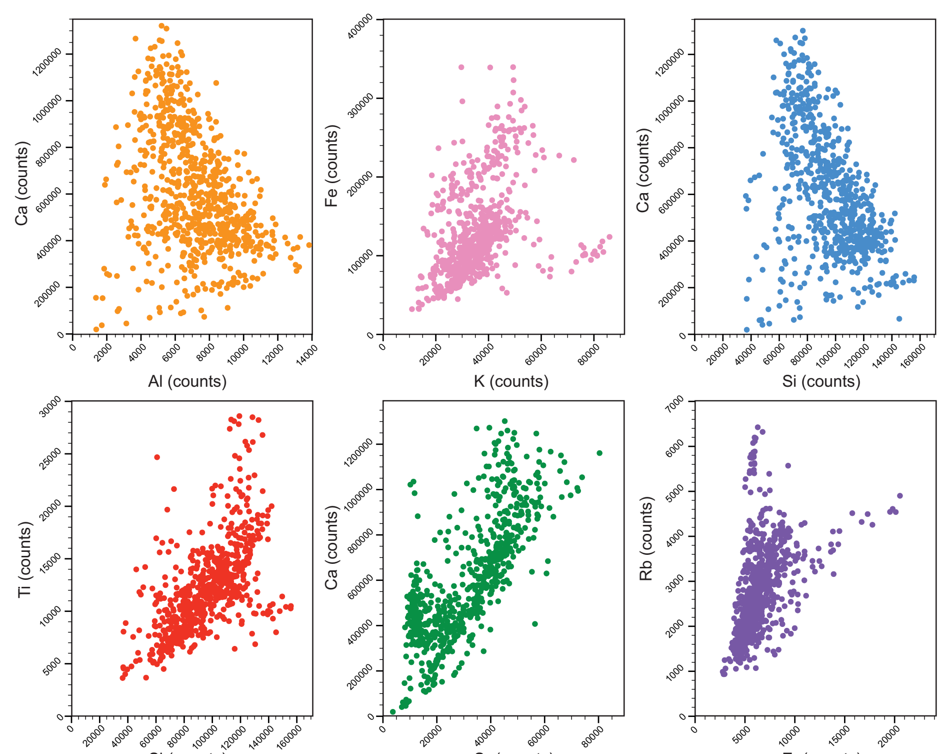

Figure F5. Crossplots of raw XRF counts for selected elements, Site U1599.

However, if instead of looking at the entirety of the splice, we zoom in on selected, more homogeneous lithologies, the correlation between elements becomes clearer. In Figure **F6**, we show the correlation of elements from a nonvolcanic ooze of Site U1599 between 417 and 534.59 m CCSF. Although the patterns are significantly closer to what would be expected from pelagic sediments (Croudace and Rothwell, 2015; Amadori et al., 2024), they are still less pronounced, owing to minor layers of volcanics and potentially bioturbation (**Druitt et al.**, 2024d).

3.3. ln(Zr/Rb)-derived grain size data

As shown for the Southern (Antarctic) Ocean (Wu et al., 2020; Ronge and Dbritto, 2024), ln(Zr/Rb) XRF data have the potential to record sortable silt–like grain sizes, assuming that Zr is usually associated with more resilient zircon minerals ($ZrSiO_4$) and Rb with minerals more prone to erosion, such as K-feldspar, mica, or clay minerals. As expected, the highly variable deposits alternating between coarse pumice layers, fine ash, and pelagic oozes make the use of XRF-derived grain sizes impossible on the level of an entire hole or site. However, if we zoom in again and only use the dolomitic marls of Lithostratigraphic Unit III (Figure **F3**), the correlation between Zr and Rb improves similar to a level expected for more pelagic sediments (Figure **F6D**; Ronge and Dbritto, 2024). We see a minor excursion in the ln(Zr/Rb) values between 565.96 and 566.56 m CCSF at Site U1591. This interval marks a section of the core that is clearly of coarser grain size than the silty clays above and below (**Druitt et al.**, 2024c). Lastly, we highlight the interval from 40.38 to 50.13 m CCSF in Site U1599. Here, we observe a rapid drop in ln(Zr/Rb) that marks a region of fine-grained oozes and mud that clearly stand out from the surrounding coarser volcanic deposits (Figure **F3**). Thus, these data indicate it might be worth investigating the use of this proxy for nonvolcanic sediments of the Aegean Sea as well.

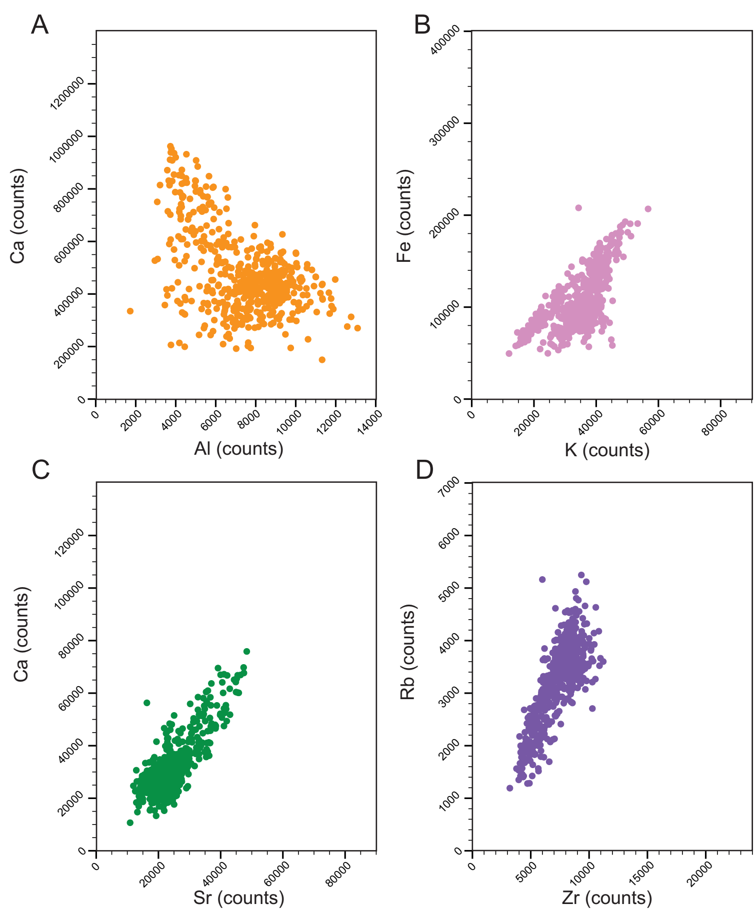

Figure F6. A–D. Crossplots of XRF counts for interval at 417–534.59 m CCSF, Site U1599. Interval is indicated in Figure F3.

4. Acknowledgments

We thank the crew, staff, and technicians of *JOIDES Resolution* Expedition 398, as well as the staff of the GCR, in particular Michelle Penkrot and Chad Broyles. We also want to thank reviewer Daniel Babin and editor Emily Estes for their comments that helped to improve this manuscript. The XRF data sets reported here are part of the Expedition 398 programmatic XRF scanning effort that was funded and supported by the National Science Foundation in agreement with the US Science Support Program (USSSP). In addition, we thank Katerina Petronotis and Brittany Stockmaster of the *JOIDES Resolution* Science Operator (JRSO), Larry Krissek of the *JOIDES Resolution* Facility Board, the US Department of State, as well as all Greek authorities involved, who made it possible to receive approval for Site U1599 in record time. We acknowledge travel support for US scientists by USSSP, as well as for European scientists by IODP-Germany and the European Consortium for Ocean Research Drilling, and the Université Clermont Auvergne in France. All data can be downloaded via the IODP Laboratory Information Management System web interface (**https://web.iodp.tamu.edu/LORE/**).

References

Amadori, C., Borrelli, C., Christeson, G., Estes, E., Guertin, L., Hertzberg, J., Kaplan, M.R., Koorapati, R.K., Lam, A.R., Lowery, C.M., McIntyre, A., Reece, J., Robustelli Test, C., Routledge, C.M., Standring, P., Sylvan, J.B., Thompson, M., Villa, A., Wang, Y., Wee, S.Y., Williams, T., Yeon, J., Teagle, D.A.H., Coggon, R.M., and the Expedition 390/393 Scientists, 2024. Data report: X-ray fluorescence scanning of sediment cores, IODP Expedition 390/393 Site U1560, South Atlantic Transect. In Coggon, R.M., Teagle, D.A.H., Sylvan, J.B., Reece, J., Estes, E.R., Williams, T.J., Christeson, G.L., and the Expedition 390/393 Scientists, South Atlantic Transect. Proceedings of the International Ocean Discovery Program, 390/393: College Station, TX (International Ocean Discovery Program). **https://doi.org/10.14379/iodp.proc.390393.205.2024**

Croudace, I.W., and Rothwell, R.G. (Eds.), 2015. Micro-XRF Studies of Sediment Cores: Applications of a Non-destructive Tool for the Environmental Sciences: Dordrecht, Netherlands (Springer). **https://doi.org/10.1007/978-94-017-9849-5**

Druitt, T., Kutterolf, S., Ronge, T.A., Hübscher, C., Nomikou, P., Preine, J., Gertisser, R., Karstens, J., Keller, J., Koukousioura, O., Manga, M., Metcalfe, A., McCanta, M., McIntosh, I., Pank, K., Woodhouse, A., Beethe, S., Berthod, C., Chiyonobu, S., Chen, H., Clark, A., DeBari, S., Johnston, R., Peccia, A., Yamamoto, Y., Bernard, A., Perez, T.F., Jones, C., Joshi, K.B., Kletetschka, G., Li, X., Morris, A., Polymenakou, P., Tominaga, M., Papanikolaou, D., Wang, K.-L., and Lee, H.-Y., 2024a. Giant offshore pumice deposit records a shallow submarine explosive eruption of ancestral Santorini. Communications Earth & Environment, 5(1):24. **https://doi.org/10.1038/s43247-023-01171-z**

Druitt, T.H., Edwards, L., Mellors, R.M., Pyle, D.M., Sparks, R.S.J., Lanphere, M., Davies, M., and Barreirio, B., 1999. Santorini Volcano. Memoir - Geological Society of London, 19. **http://pubs.er.usgs.gov/publication/70094778**

Druitt, T.H., Kutterolf, S., Ronge, T.A., Beethe, S., Bernard, A., Berthod, C., Chen, H., Chiyonobu, S., Clark, A., DeBari, S., Fernandez Perez, T.I., Gertisser, R., Hübscher, C., Johnston, R.M., Jones, C., Joshi, K.B., Kletetschka, G., Koukousioura, O., Li, X., Manga, M., McCanta, M., McIntosh, I., Morris, A., Nomikou, P., Pank, K., Peccia, A., Polymenakou, P.N., Preine, J., Tominaga, M., Woodhouse, A., and Yamamoto, Y., 2024b. Expedition 398 summary. In Druitt, T.H., Kutterolf, S., Ronge, T.A., and the Expedition 398 Scientists, Hellenic Arc Volcanic Field. Proceedings of the International Ocean Discovery Program, 398: College Station, TX (International Ocean Discovery Program). **https://doi.org/10.14379/iodp.proc.398.101.2024**

Druitt, T.H., Kutterolf, S., Ronge, T.A., Beethe, S., Bernard, A., Berthod, C., Chen, H., Chiyonobu, S., Clark, A., DeBari, S., Fernandez Perez, T.I., Gertisser, R., Hübscher, C., Johnston, R.M., Jones, C., Joshi, K.B., Kletetschka, G., Koukousioura, O., Li, X., Manga, M., McCanta, M., McIntosh, I., Morris, A., Nomikou, P., Pank, K., Peccia, A., Polymenakou, P.N., Preine, J., Tominaga, M., Woodhouse, A., and Yamamoto, Y., 2024c. Site U1591. In Druitt, T.H., Kutterolf, S., Ronge, T.A., and the Expedition 398 Scientists, Hellenic Arc Volcanic Field. Proceedings of the International Ocean Discovery Program, 398: College Station, TX (International Ocean Discovery Program). **https://doi.org/10.14379/iodp.proc.398.105.2024**

Druitt, T.H., Kutterolf, S., Ronge, T.A., Beethe, S., Bernard, A., Berthod, C., Chen, H., Chiyonobu, S., Clark, A., DeBari, S., Fernandez Perez, T.I., Gertisser, R., Hübscher, C., Johnston, R.M., Jones, C., Joshi, K.B., Kletetschka, G., Koukousioura, O., Li, X., Manga, M., McCanta, M., McIntosh, I., Morris, A., Nomikou, P., Pank, K., Peccia, A., Polymenakou, P.N., Preine, J., Tominaga, M., Woodhouse, A., and Yamamoto, Y., 2024d. Site U1599. In Druitt, T.H., Kutterolf, S., Ronge, T.A., and the Expedition 398 Scientists, Hellenic Arc Volcanic Field. Proceedings of the International Ocean Discovery Program, 398: College Station, TX (International Ocean Discovery Program). **https://doi.org/10.14379/iodp.proc.398.113.2024**

Druitt, T.H., and Vougioukalakis, G.E. (Eds.), 2019. South Aegean Volcanic Arc. Elements, 15(3). **https://www.elementsmagazine.org/south-aegean-volcanic-arc/**

Hsü, K.J., 1987. The Mediterranean was a Desert: A Voyage of the Glomar Challenger: Princeton, NJ (Princeton University Press).

Loughlin, S.C., Sparks, S., Brown, S.K., Jenkins, S.F., and Vye-Brown, C. (Eds.), 2015. Global Volcanic Hazards and Risk: Cambridge (Cambridge University Press). **https://doi.org/10.1017/CBO9781316276273**

Penkrot, M.L., Jaeger, J.M., Cowan, E.A., St-Onge, G., and LeVay, L., 2018. Multivariate modeling of glacimarine lithostratigraphy combining scanning XRF, multisensory core properties, and CT imagery: IODP Site U1419. Geosphere, 14(4):1935–1960. **https://doi.org/10.1130/GES01635.1**

Preine, J., Hübscher, C., Karstens, J., and Nomikou, P., 2022. Volcano-tectonic evolution of the Christiana-Santorini-Kolumbo rift zone. Tectonics, 41(11):e2022TC007524. **https://doi.org/10.1029/2022TC007524**

Preine, J., Karstens, J., Hübscher, C., Druitt, T., Kutterolf, S., Nomikou, P., Manga, M., Gertisser, R., Pank, K., Beethe, S., Berthod, C., Crutchley, G., McIntosh, I., Ronge, T., Tominaga, M., Clark, A., DeBari, S., Johnston, R., Mateo, Z., Peccia, A., Jones, C., Kletetschka, G., Metcalfe, A., Bernard, A., Chen, H., Chiyonobu, S., Fernandez-Perez, T., Joshi, K.B., Koukousioura, O., McCanta, M., Morris, A., Polymenakou, P., Woodhouse, A., Yamamoto, Y., Wang, K.-L., Lee, H.-Y., Li, X., and Papanikolaou, D., 2024. Hazardous explosive eruptions of a recharging multi-cyclic island arc caldera. Nature Geoscience. **https://doi.org/10.1038/s41561-024-01392-7**

Ronge, T.A., and Dbritto, S., 2024. Data report: using XRF scanning–derived grain size analysis for rapid assessment of bottom current velocities on long drill cores from the southern Scotia Sea, IODP Expedition 382. In Weber, M.E., Raymo, M.E., Peck, V.L., Williams, T., and the Expedition 382 Scientists, Iceberg Alley and Subantarctic Ice and Ocean Dynamics. Proceedings of the International Ocean Discovery Program, 382: College Station, TX (International Ocean Discovery Program). **https://doi.org/10.14379/iodp.proc.382.201.2024**

Ryan, W.B.F., Carbotte, S.M., Coplan, J.O., O'Hara, S., Melkonian, A., Arko, R., Weissel, R.A., Ferrini, V., Goodwillie, A., Nitsche, F., Bonczkowski, J., and Zemsky, R., 2009. Global multi-resolution topography synthesis. Geochemistry, Geophysics, Geosystems, 10(3):Q03014. **https://doi.org/10.1029/2008GC002332**

Taylor, S.P., Patterson, M.O., Lam, A.R., Jones, H., Woodard, S.C., Habicht, M.H., Thomas, E.K., and Grant, G.R., 2022. Expanded North Pacific subtropical gyre and heterodyne expression during the Mid-Pleistocene. Paleoceanography and Paleoclimatology, 37(5):e2021PA004395. **https://doi.org/10.1029/2021PA004395**

Vasiliev, M.A., Blum, P., Chubarian, G., Olsen, R., Bennight, C., Cobine, T., Fackler, D., Hastedt, M., Houpt, D., Mateo, Z., and Vasilieva, Y.B., 2011. A new natural gamma radiation measurement system for marine sediment and rock analysis. Journal of Applied Geophysics, 75(3):455–463. **https://doi.org/10.1016/j.jappgeo.2011.08.008**

Wu, L., Wilson, D.J., Wang, R., Yin, X., Chen, Z., Xiao, W., and Huang, M., 2020. Evaluating Zr/Rb ratio from XRF scanning as an indicator of grain-size variations of glaciomarine sediments in the Southern Ocean. Geochemistry, Geophysics, Geosystems, 21(11):e2020GC009350. **https://doi.org/10.1029/2020GC009350**